Full length article

The promotional effect of H_2 reduction treatment on the low-temperature NH_3-SCR activity of Cu/SAPO-18

Na Zhu[a,b], Zhihua Lian[a], Yan Zhang[a,c], Wenpo Shan[a,c,*], Hong He[a,b,c,d]

[a] *Center for Excellence in Regional Atmospheric Environment and Key Laboratory of Urban Pollutant Conversion, Institute of Urban Environment, Chinese Academy of Sciences, Xiamen 361021, China*
[b] *University of Chinese Academy of Sciences, Beijing 100049, China*
[c] *Ningbo Urban Environment Observation and Research Station-NUEORS, Institute of Urban Environment, Chinese Academy of Sciences, Ningbo 315800, China*
[d] *State Key Joint Laboratory of Environment Simulation and Pollution Control, Research Center for Eco-Environmental Sciences, Chinese Academy of Sciences, Beijing 100085, China*

A B S T R A C T

In this study, a Cu/SAPO-18 catalyst was treated by H_2 reduction, which induced a remarkable enhancement of the low-temperature NH_3-SCR activity. Compared with the fresh catalyst, the reduced Cu/SAPO-18 catalyst showed an increase in NO_x conversion from 45% to 80% at 175 °C, and from 80% to 100% at 200 °C, under a GHSV of 200,000 h^{-1}. The characterization (XRD, XPS and H_2-TPR) and in-situ DRIFTS results confirmed that a large amount of Cu cations (most of which were Cu^+ ions) existed on/in Cu/SAPO-18 after the H_2 reduction treatment. The increased Cu^+/Cu^{2+} ratio led to the enhanced low-temperature SCR activity.

1. Introduction

The selective catalytic reduction of NO_x with ammonia (NH_3-SCR) has been widely used to abate nitrogen oxides emitted into the atmosphere from stationary and mobile sources [1,2]. The commercial NH_3-SCR catalyst system is mainly V_2O_5-WO_3 (MO_3)/TiO_2. However, there are still some inevitable disadvantages in the application of this system, such as a narrow operating temperature window, low N_2 selectivity in the high-temperature range, and the toxicity of the active vanadium species. Recently, many studies have been focused on the development of vanadium-free oxide catalysts, such as Fe- or Ce-based oxide catalysts (Fe−Ti [3], Ce−Ti [4,5], Ce-W-Ti [6], Ce−Zr [7,8]) with superior middle/high-temperature SCR activity, and Mn- or Cu-based oxide catalysts (Mn−Ti [9], Mn-Ce-Ti [10], $MnWO_x$ [11], CuO_x/TiO_2 [12], CuO_x/WO_3-ZrO_2 [13]) with excellent low-temperature performance.

Currently, metal-promoted zeolite catalysts, especially Cu and Fe-zeolite catalysts, have attracted considerable interest for their excellent catalytic activity and relatively broad operating temperature window of high de-NO_x efficiency [14–17]. In particular, Cu-based small-pore chabazite (CHA) structure zeolites (such as Cu-SSZ-13) have been intensely investigated due to their excellent SCR activity and exceptional hydrothermal stability [18–26]. Many studies have focused on the activity, SO_2 resistance, and the nature of the active Cu species in Cu-SSZ-

13 [27–31]. Besides Cu-exchanged CHA, another type of small pore zeolite with AEI framework topology (e.g. Cu-SSZ-39) was also reported to be an efficient and stable catalyst for NH_3-SCR [32,33]. Moliner et al. reported that Cu-SSZ-39 showed better catalytic performance than commercial Cu-SSZ-13 [32]. SAPO-18 and its analogs, which are aluminosilicophosphates with the AEI structure, have been widely used in the methanol-to-olefin (MTO) reaction in the past decades [34,35]. Recently, Cu-SAPO-18 catalysts have been recognized as some of the most promising candidates for NH_3-SCR, due to their excellent activity and high hydrothermal stability [36–39]. Li et al. synthesized CeO_2-protected Cu-SAPO-18 catalysts, which exhibited high H_2O and SO_2 resistance in NH_3-SCR [40].

Previous studies showed that CuO_x species (including Cu dimers, Cu oligomers or Cu clusters) clearly coexisted with isolated Cu^{2+} ions in the Cu-SAPO-34 catalysts, even at very low Cu loading [41–44]. CuO_x did not contribute to the SCR activity in the low temperature range, and decreased the activity in the high temperature range seriously due to the unselective oxidation of NH_3 [42,45]. Thus, elimination of CuO_x species is necessary to improve SCR performance. Previous studies also showed that the SCR activity of Fe-ZSM-5 and Fe-Beta can be improved by high-temperature hydrogen treatment of the sample, due to breaking up iron oxide clusters into smaller iron species and forming stronger bonds to the zeolite matrix [46–48]. In addition, Shwan et al. reported

that copper could be ion-exchanged into CHA zeolite by exposing copper oxides and zeolite to the NH$_3$-SCR atmosphere at 250 °C, and the Cu ion-exchange was related to the formation of Cu$_2$O [49]. Therefore, it should be confirmed whether CuO$_x$ species in/on Cu/SAPO-18 could be reduced to Cu$^+$ by H$_2$ at low temperature and then ion-exchanged into the zeolite under the NH$_3$-SCR atmosphere. To the best of our knowledge, no studies about this treatment of Cu-based zeolite have been reported.

In the present work, Cu/SAPO-18 was prepared using a simple wetness impregnation method and treated by H$_2$ reduction and subsequent SCR treatment. It was found that the H$_2$-reduced catalysts yielded significantly enhanced low-temperature SCR activity, compared with the untreated Cu/SAPO-18. This opens a new route for improving the low-temperature activity of Cu-promoted zeolite catalysts.

2. Experimental

2.1. Catalyst preparation

SAPO-18 templated by N, N-diisopropylethylamine (DIEA) was hydrothermally synthesized, with the starting gel composition of 1.6 DIEA/1.0 Al$_2$O$_3$/0.9 P$_2$O$_5$/0.6 SiO$_2$/50 H$_2$O [50]. The gel mixture was stirred for about 3 h at room temperature and then transferred into a 100 mL Teflon-lined stainless steel autoclave. The crystallization was performed at 180 °C for 96 h under autogenous pressure without agitation. After crystallization, the obtained mixture was washed by deionized water repeatedly with centrifugation. Finally, the solid was dried at 100 °C overnight and calcined at 550 °C for 5 h in a muffle furnace with a heating rate of 5 °C/min to obtain the template-free samples.

Cu/SAPO-18 was prepared via a wet impregnation method. Cu (NO$_3$)$_2$·3H$_2$O was dissolved in deionized water and mixed with the synthesized SAPO-18 zeolite powders. The precursor was continuously and thoroughly stirred for 1 h, then ultrasonically treated for 0.5 h. The liquid phase obtained was then dried at 60 °C using a rotary evaporator employing a vacuum pump. Afterwards, the powders were dried at 100 °C overnight and calcined at 550 °C for 4 h in a muffle furnace.

Cu/SAPO-18-R was obtained by treating the Cu/SAPO-18 in 5% vol. H$_2$/N$_2$ at 250 °C for 5 h, and then exposing it to the NH$_3$-SCR atmosphere according to the activity test procedure. The reason for the treatment under the NH$_3$-SCR atmosphere was to promote exchange of the reduced Cu$^+$ into the zeolite and stabilize the catalyst in an oxidizing environment.

2.2. Characterization

The actual content of Cu, Si, Al and P in the catalysts was analyzed using an inductively coupled plasma instrument (OPTIMA 7000DV) with a radial view of the plasma. All samples were dissolved using strong acid solution before the test.

The morphology of the samples was observed by scanning electron microscopy (SEM) using a S4800 electron microscope.

The surface area and pore characteristics of the catalysts were obtained from N$_2$ adsorption/desorption analysis at −196 °C using a physisorption analyzer (Quantachrome). Prior to the N$_2$ physisorption, the catalysts were degassed at 250 °C for 6 h. Surface area was determined by the BET equation in the 0.05–0.35 partial pressure range.

Powder X-ray diffraction (XRD) measurements were recorded on a computerized PANalytical X pert Pro diffractometer with Cu Kα radiation. The data of 2θ from 0° to 50° were collected with the step size of 0.02. The small angle X-ray scattering data of 2θ from 1° to 10° were collected with the step size of 0.006.

The H$_2$-TPR experiments were performed on a ChemStar chemisorption analyzer (Quantachrome). The samples (50 mg) were pretreated in a quartz reactor at 500 °C in a flow of air (50 mL/min) for 1 h and cooled down to room temperature. Then H$_2$-TPR was performed

from room temperature to 800 °C in 10 vol% H$_2$/Ar gas flow of 50 mL/min at a heating rate of 10 °C/min.

The EPR spectra were obtained using a Bruker EMX spectrometer (USA) at 90 K. For measurement, powder samples (30 mg) were placed into quartz tubes and sealed with a plastic cover.

The X-ray photoelectron spectroscopy (XPS) measurements were carried out with a scanning X-ray microprobe (EScalab 250, Thermo Fisher Scientific) using Al Kα radiation (1486.6 eV). All the binding energies were calibrated using the C1s peak (BE = 284.6 eV) as standard.

In situ DRIFTS experiments were performed on an FTIR spectrometer (Nicolet IS50 FT-IR) equipped with a Smart Collector and an MCT/A detector cooled by liquid nitrogen. The reaction temperature was controlled precisely by an Omega programmable temperature controller. The catalyst was pretreated in 20% O$_2$/N$_2$ flow at 300 °C for 30 min, and then purged with N$_2$ until it cooled down to 75 °C. For NH$_3$ adsorption, the sample was exposed to a flow of 500 ppm NH$_3$/N$_2$ for 1 h and then purged by N$_2$. All spectra were recorded by accumulating 100 scans with a resolution of 4 cm^{-1}.

2.3. Activity measurements

Before NH$_3$-SCR activity tests, the catalysts were pressed, crushed and sieved to 40–60 mesh. The SCR activity tests were carried out in a fixed-bed quartz flow reactor at atmospheric pressure. The reaction conditions were controlled as follows: 500 ppm NO, 500 ppm NH$_3$, 5 vol% O$_2$ and N$_2$ balance. Under ambient conditions, the total flow rate was 500 mL/min and the gas hourly space velocity (GHSV) was 200,000 h^{-1}. The concentrations of N-containing gases (NO, NH$_3$, NO$_2$, and N$_2$O) in the effluent were continuously analyzed by a gas analyzer (Antaris IGS, Thermo Fisher) equipped with a heated, low-volume multiple-path gas cell. The FTIR spectra were collected throughout and the results were recorded when the SCR reaction reached a steady state.

3. Results and discussion

3.1. Catalytic performance

The NO$_x$ conversion as a function of temperature for the standard SCR reaction at a GHSV of 200,000 h^{-1} over the fresh and H$_2$ treated samples are both shown in Fig. 1. The Cu/SAPO-18 catalyst showed high SCR activity, with NO$_x$ conversion above 80% in the temperature range of 200–375 °C. After H$_2$ reduction treatment and subsequent exposure to the NH$_3$-SCR atmosphere, Cu/SAPO-18-R showed remarkably improved low-temperature activity, with NO$_x$ conversion increased
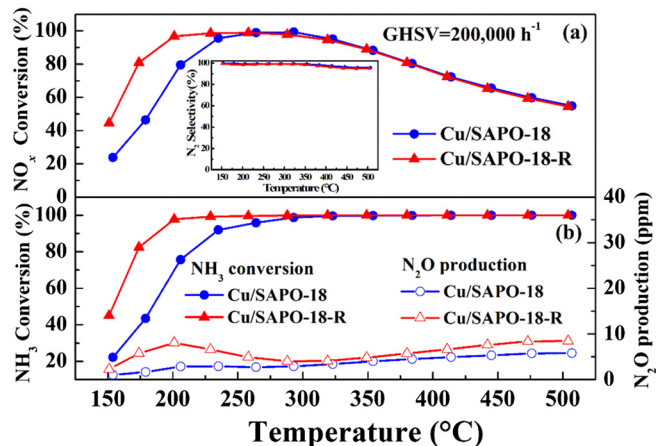

Fig. 1. NH$_3$-SCR performance of different Cu/SAPO-18 catalysts. Reaction conditions: [NO] = [NH$_3$] = 500 ppm, [O$_2$] = 5 vol%, N$_2$ balance, and GHSV = 200,000 h^{-1}.

from 45% to 80% at 175 °C, and from 80% to 100% at 200 °C. It should be noted that, Cu/SAPO-18 was treated by SCR atmosphere only, the activity did not show any significant change. When Cu/SAPO-18 was reduced by H_2 only, the low-temperature activity enhanced but high-temperature activity decreased. However, when Cu/SAPO-18 was reduced by H_2 and then exposed to SCR atmosphere, the low-temperature enhanced and high-temperature activity recovered to the original level (Cu/SAPO-18) (Fig. S1). In this study, hydrogen treatment and SCR treatment are two key successive steps for this sample system. The low-temperature activity was enhanced, which may be due to the change of the Cu active species, and this will be discussed in the subsequent characterization sections. In addition, the N_2 selectivity of Cu/SAPO-18 and Cu/SAPO-18-R catalysts maintained at a level of over 90% in the whole temperature range. The low-temperature NH_3 conversion of Cu/SAPO-18-R was obviously higher than that of Cu/SAPO-18, due to its higher SCR activity. The N_2O productions over the catalysts were lower than 10 ppm in the whole temperature range, with the production over Cu/SAPO-18-R slightly higher than that over Cu/SAPO-18.

3.2. Characterization of the catalyst

3.2.1. Structure of the catalysts investigated by BET, XRD, SEM and EPR

The results of N_2 physisorption in Table 1 illustrate that the specific surface areas and accumulated pore volumes decreased after the impregnation of the H-SAPO-18 zeolite support with copper, which may be associated with CuO_x species blocking the pores of the zeolite. Compared with Cu/SAPO-18, the specific surface area and pore volume of Cu/SAPO-18-R decreased slightly, which may be due to the migration and transformation of Cu species, as explained in the subsequent sections.

The elemental content of the samples is shown in Table 1. According to the Si substitution, in theory the acidity of SAPO-18 comes from the substitution of P by Si. Cu ions can only locate at the acid sites of the SAPO-18 support. The Si islands cannot generate acid sites. The molar ratio of (Si + P) / Al is bigger than 1, indicating that Si atoms substitute for P and Al to form the Si islands in Cu/SAPO-18 catalysts [51]. ICP results revealed that the content of copper was about 3.7%, and the Cu/Al ratio was 0.1, indicating that CuO_x species may be formed due to the excess of Cu^{2+} species and insufficient acid sites [52].

The XRD (2θ = 0–50°) profiles in Fig. 2a show the presence of the typical AEI structure in the two samples, suggesting that the incorporation of copper and H_2-reduction treatment did not affect the zeolite structure. The slight decline of the peak intensities of Cu/SAPO-18 may be due to lower crystallinity, resulting from the partial collapse of the micropore structure, which was consistent with the BET results. On the other hand, CuO_x species (CuO, Cu dimers or Cu oligomers) were not detected, which may be due to their high dispersion on/in the zeolite.

In order to detect the copper incorporated into the SAPO-18 crystal lattice, the XRD patterns in the range of 1–10° are shown in Fig. 2b. After the introduction of copper, the interplanar crystal spacing of (110) (noted as 'd') increased measurably from 9.2210 to 9.3165, indicating that copper ions were exchanged into the zeolite and resulted in crystal lattice deformation. The 'd' value of Cu/SAPO-18-R shifted to
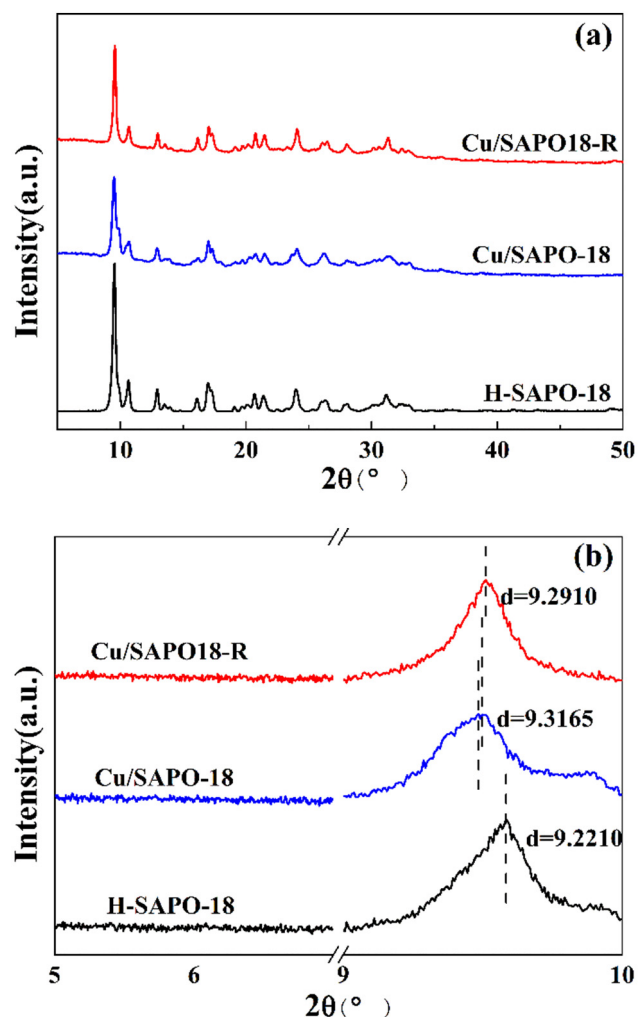

Fig. 2. XRD profiles (2θ = 0–50°) (a) and XRD profiles (2θ = 1–10°) (b) of the Cu/SAPO-18 catalysts.

9.2910, which may be owing to the migration and relocation of the copper species in the zeolite. It indicated the decrease of lattice deformation for Cu/SAPO-18-R, which may be a reason for the higher peak intensity of Cu/SAPO-18-R than that of Cu/SAPO-18.

The SEM images in Fig. 3 show that all the samples had similar morphologies, which consisted of square-platelet crystals (typical SAPO-18 crystal) [50] and a trace amount of cubic structure (SAPO-34 impurity phase). However, lots of debris could be seen in the SEM images of these samples, which demonstrated that the crystal form of SAPO-18 synthesized by this method was not perfect.

EPR is an excellent technique for identifying the coordination environment of isolated Cu^{2+} ions, because all the other Cu species ([Cu-O-Cu]$^{2+}$ or Cu$^+$) are EPR silent [18]. The EPR spectra along with 'g' and 'A' values of two Cu/SAPO-18 catalysts are shown in Fig. 4. The 'g'

Table 1
Textural properties and elemental content of the samples.

Samples	A_{BET}[a] (m²/g)	V[b] (cm³/g)	Si/Al[c] molar ratio	(Si + P)/Al[c] molar ratio	Cu content (%)[c]	Cu/Al[c] molar ratio
H-SAPO-18	558	0.38	0.57	1.42	–	–
Cu/SAPO-18	503	0.30	0.57	1.38	3.7	0.1
Cu/SAPO-18-R	481	0.28	0.57	1.38	3.7	0.1

[a] A_{BET}[a] is the BET surface area calculated by the BET method.
[b] V[b] is the total pore volume at p/p₀ = 0.99.
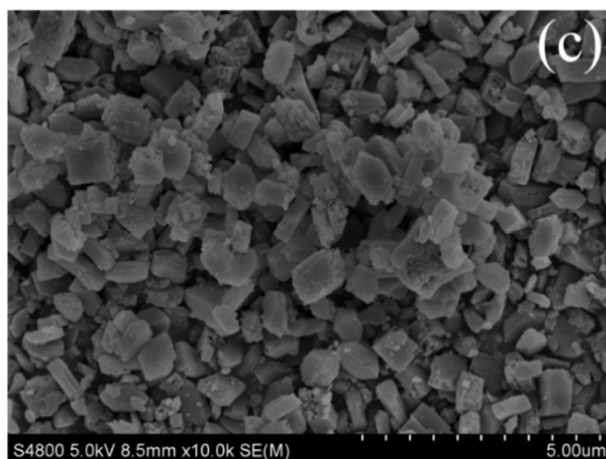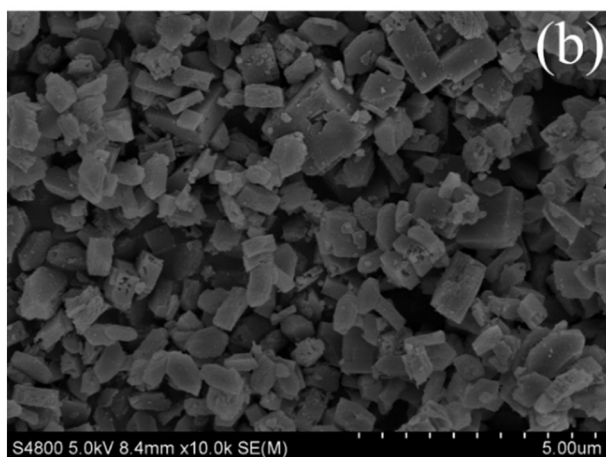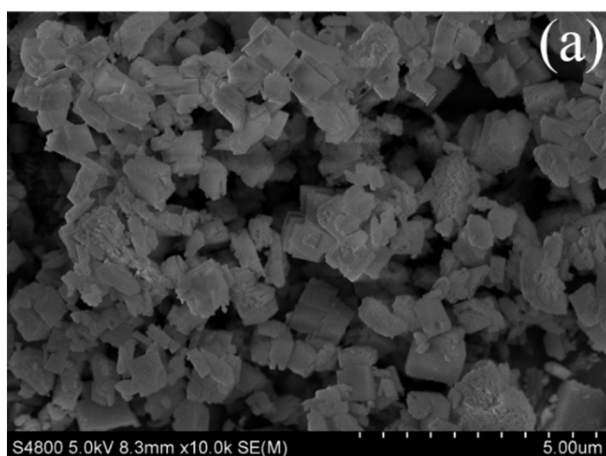[c] ICP results.

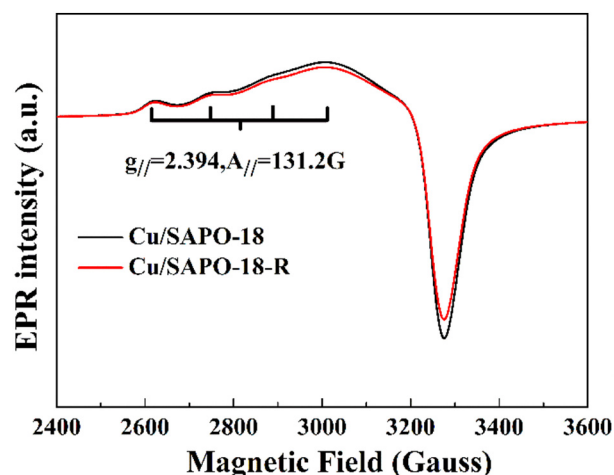Fig. 3. SEM images of H-SAPO-18 (a), Cu/SAPO-18 (b) and Cu/SAPO-18-R (c).

Fig. 4. EPR spectra of Cu/SAPO-18 catalysts.

site I in the Cu-CHA structure [45,52]. The intensity of the EPR signal of Cu/SAPO-18-R decreased, indicating that the content of Cu^{2+} ions in Cu/SAPO-18-R declined due to the reduction of some Cu^{2+} ions to Cu^{+} during the H_2 reduction process.

3.2.2. H_2-TPR results

H_2-TPR was used to characterize the reducibility of various copper species in the samples. No clear H_2 consumption signal was observed for the H-SAPO-18 sample, and the TPR curve of H-SAPO-18 could be used as the baseline for the Cu/SAPO-18 samples. H_2-TPR is an effective method to distinguish Cu dimers and CuO clusters from isolated Cu^{2+} due to the more facile reduction of the former species. Fig. 5a depicts the H_2-TPR curves of all the catalysts. The amount of H_2 consumption decreased when Cu/SAPO-18 was treated by H_2 reduction followed by the SCR atmosphere, which may be because some Cu species (e.g. Cu dimers) were reduced to Cu^{+}, or a fraction of Cu^{2+} was reduced to Cu^{+}. For both Cu/SAPO-18 and Cu/SAPO-18-R, H_2 consumption profiles could be more accurately divided into four peaks after a peak fitting process based on the Gaussian-Lorenz deconvolution method, as shown in Fig. 5b.

In previous studies, the one-step reduction of dispersed bulk CuO to Cu^0 occurred in the temperature range of 300–310 °C [43,45,54]. However, the surface Cu clusters and Cu dimers $[Cu-O-Cu]^{2+}$ were easier to reduce than bulk CuO below 250 °C [52]. Thus, the peak at 215 °C may be assigned to the overlap of peaks for the reduction of surface Cu clusters to Cu^0 and Cu dimers to Cu^{+}. The reduction of Cu^{2+} ions in zeolites followed a two-step process, which included the reduction from Cu^{2+} to Cu^{+} (at low temperature) and the reduction from Cu^{+} to Cu^0 (at high temperature). Three types of isolated Cu ions could exist in Cu-zeolites: Cu^{2+} ions that balance two negative framework charges, and $[Cu^{2+}(OH)]^{+}$ and Cu^{+} species that balance one negative charge. Cu^{2+} ions may occupy sites next to faces of 6-membered rings (site A), and $[Cu^{2+}(OH)]^{+}$ may occupy sites within the CHA cages, likely next to 8-membered rings (site B). The two different types of Cu^{2+} had different reducibility, and the latter was more easily reduced [36,52,54,55]. Therefore, the peaks at 240–260 °C could be assigned to the reduction of highly stable Cu^{2+} ions to Cu^{+} ions (site A). The peaks at 167 °C could be assigned to the reduction of less-stable Cu^{2+} ions to Cu^{+} ions (site B). The facile reducibility of these less-stable Cu^{2+} ions could be responsible for the excellent NH_3-SCR performance of the catalysts at low temperature [25]. The broad peaks at 395 °C for Cu/SAPO-18 and 351 °C for Cu/SAPO-18-R could be assigned to the reduction of the low-stability Cu^{+} to Cu^0, respectively. The peak at 538 °C for the Cu/SAPO-18 catalyst and the peak at 545 °C for Cu/SAPO-18-R could be attributed to the reduction of highly stable Cu^{+} ions to Cu^0.

On the basis of the deconvolution results, the temperature of

and 'A' values are usually used to identify the coordination environment of Cu^{2+} ions. For Cu/SAPO-18 and Cu/SAPO-18-R samples, axially symmetrical signals were observed with hyperfine splitting originating from the copper with nuclear spin 3/2. By analyzing the hyperfine features, $g_{||} = 2.394 \pm 0.002$ and $A_{||} = 131.2$ G were obtained. These values are consistent with an octahedral state for the hydrated samples, in which the Cu^{2+} is octahedrally coordinated to three framework oxygen and three water molecules [41,53]. Isolated Cu^{2+} ions in hydrated SAPO-18 were displaced from the six-membered ring into the ellipsoidal cavity, which seemed similar to the so-called

(a)

Fig. 6. Cu 2p XPS spectra of Cu/SAPO-18 catalysts.

3.2.3. XPS results

XPS was used to detect the surface copper species present in these catalysts. The binding energy of the Cu 2p transition peaks provided information on the state of Cu species on the surface. As shown in Fig. 6, two shake-up satellite peaks corresponding to Cu^{2+} appeared at about 943 and 963 eV. These characteristic satellite peaks could be attributed to the charge transfer between the transition metal 3d orbitals and surrounding ligand oxygen 2p orbitals, and which could be used to distinguish between Cu^{2+} and Cu^+ or Cu^0 species [36,44]. The Gaussian-Lorentz fit to Cu $2p_{3/2}$ indicated that the main peaks were composed of two peaks at 933.2 and 935.7 eV, respectively. The peak at 935.7 eV corresponds to the Cu^{2+} ions coordinated to framework oxygen atoms of SAPO-18 zeolite [44,56]. In order to accurately determine the valence of Cu, it was essential to refer to the Auger parameters of different species [57]. Generally, the distinction was made by using amended Auger parameters 'a' ($a = E_k$ (Cu L_3VV) + E_b (Cu $2p_{3/2}$)), and the results are shown in Table 3. At the binding energy of 933.2 eV on the surface of the two samples, Cu atoms, whose Auger parameters 'a' were both 1847.1 eV, existed mainly in the form of Cu^+.

The surface atomic concentration and the amount of each Cu species (based on integration of peak areas) for the two samples are listed in Table 3. The Si/Al ratio on the surface of Cu/SAPO-18-R was lower than that of Cu/SAPO-18, which indicated that Al was enriched on the surface after the H_2 reduction treatment. It should be noted that, the charge-compensated Cu dimers was reduced by hydrogen treatment, which could result in the formation of partial extra-framework Al species. The increase of Al concentration on Cu/SAPO-18-R surface may be due to the migration of extra-framework Al species to surface under the effect of H_2O, which was produced during the reduction of Cu
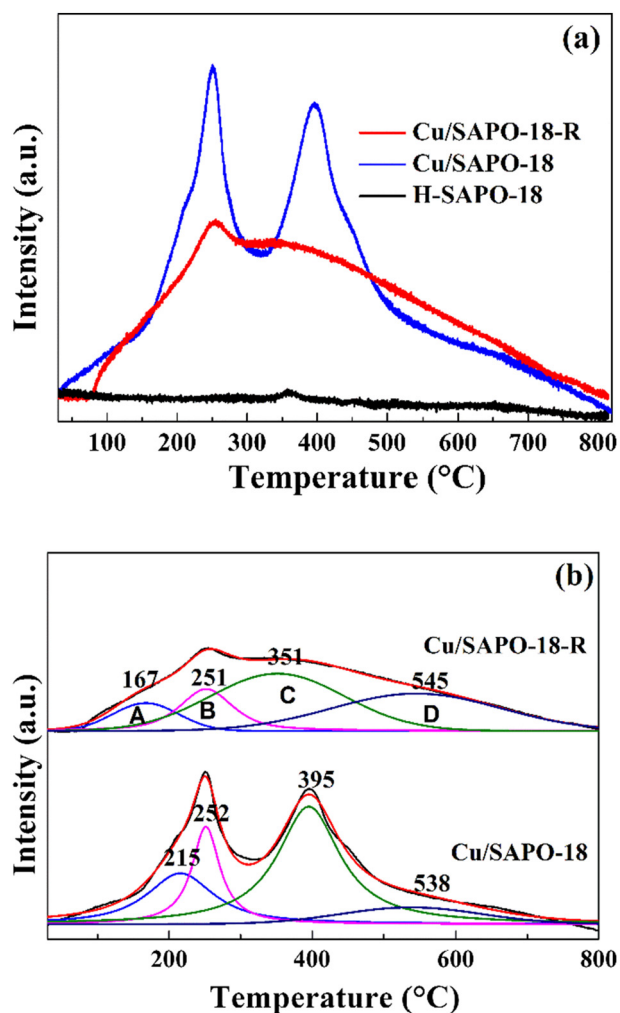

(b)

Fig. 5. H_2-TPR profiles of Cu/SAPO-18 catalysts.

Table 2
Temperature and H_2 consumption ratio related with the H_2-TPR profiles of the catalysts by Gaussian-Lorenz deconvolution.

Samples	Temperature (°C) and H_2 consumption ratio (%)[a]							
	Peak A		Peak B		Peak C		Peak D	
	(Site B) Cu^{2+} or Cu cluster to Cu^+ or Cu^0		(Site A) Cu^{2+} to Cu^+		Low stable Cu^+ to Cu^0		High stable Cu^+ to Cu^0	
Cu/SAPO-18	215	20.9	252	18.9	395	49.0	538	11.2
Cu/SAPO-18-R	167	9.9	251	14.7	351	41.6	545	33.7

[a] Integral areas ratio of H_2 consumption in terms of Gaussian-Lorenz deconvolution using Peakfit instrument.

reduction peaks and the H_2 consumption of the related Cu species were determined and listed in Table 2. Apparently, for both the samples, the total H_2 consumption of peaks C and D was always stronger than that of peaks A and B, because the H_2 consumption (peaks C and D) of Cu^+ included that for the reduction of isolated Cu^{2+} ions and the original Cu^+ ions existing in the framework of the zeolite. It was considered that there were two kinds of original Cu^+ ions coordinated with the zeolite framework [54], which was consistent with our present observation, including the low-stability Cu^+ ions and high-stability Cu^+ ions. It was observed that the total amount of original Cu^+ ions in Cu/SAPO-18-R was higher than that of Cu/SAPO-18. This may be the reason that the low-temperature activity was enhanced after H_2-reduction treatment.
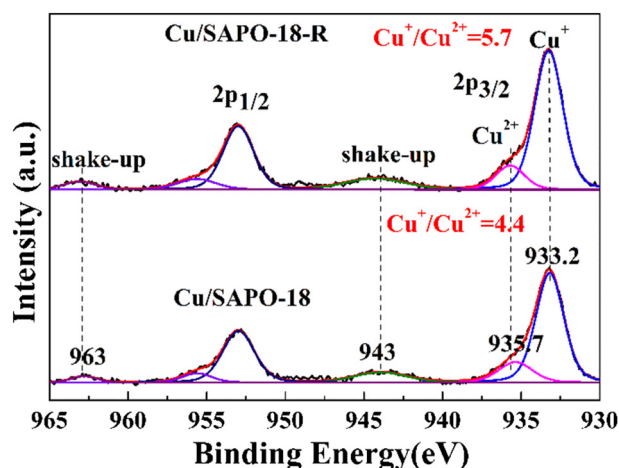
Table 3
XPS elemental analysis and integrated areas of Cu $2p_{3/2}$ XPS peaks for different Cu species on Cu/SAPO-18 catalysts.

Samples	Surface atomic concentration/mol %							
	Al 2p	Si 2p	P 2p	O 1s	Cu 2p	Si/Al	Cu/Al	Cu/wt%[a]
Cu/SAPO-18	15.95	13.36	9.60	59.79	1.30	0.84	0.08	3.87
Cu/SAPO-18-R	17.11	10.76	11.07	59.65	1.41	0.63	0.08	4.17

	E_b (eV)	E_k (eV)	a (Cu) (eV)	Cu^{+b}	Cu^{2+b}
Cu/SAPO-18	933.2	913.9	1847.1	7729.7	1767.9
Cu/SAPO-18-R	933.2	913.9	1847.1	9675.7	1692.7

[a] Superficial Cu content: Cu/wt% = [MCu/M(Cu + Al + Si + O)] × 100.
[b] Integrated areas of Cu $2p_{3/2}$ peaks in terms of Gaussian-Lorenz deconvolution using Peakfit software.
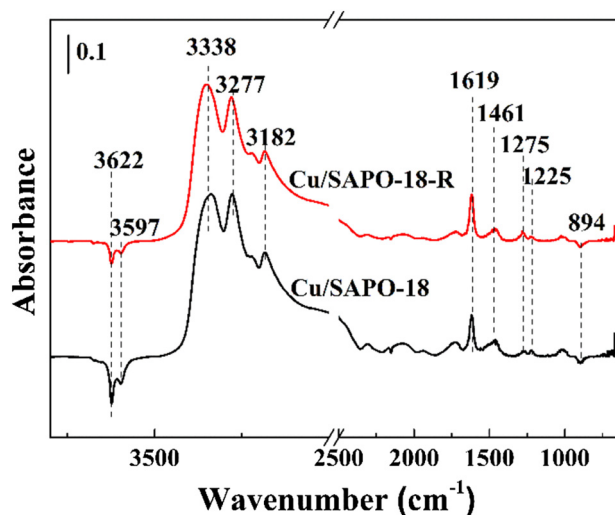
Fig. 7. In situ DRIFTS of NH_3 adsorption at 75 °C.

dimers by H_2 [58]. It was confirmed that the negative charge of the framework could affect the location of Cu species. Therefore, the surface Cu wt% calculated from XPS data for Cu/SAPO-18-R was 4.17%, which was higher than that of Cu/SAPO-18.

Furthermore, the amount of Cu^+ ions increased and Cu^{2+} ions decreased after the H_2 reduction treatment and subsequent SCR treatment, and the Cu^+/Cu^{2+} ratio of Cu/SAPO-18-R (5.7%) was higher than that of Cu/SAPO-18 (4.4%). The SCR treatment after H_2 reduction could influence Cu^+ generation, and the corresponding XPS results of Cu/SAPO-18 with H_2 treatment only were shown in Fig. S2.

3.3. NH_3 adsorption results

In-situ DRIFTS experiments were used to characterize the different acid sites. NH_3 was used as a probe molecule since NH_3 could absorb on both Brønsted acid sites and Lewis acid sites of the zeolite material. Therefore, the relative intensities of the DRIFTS features after NH_3 saturation were indicative of the total amounts of different acid sites. NH_3 adsorption experiments were carried out at 75 °C. The obtained spectra are shown in Fig. 7.

Generally, the features at high wavenumbers ($> 3000\,cm^{-1}$) originated from the stretching vibrations of the N−H bonds, and the features in the low wavenumber region ($1400–1650\,cm^{-1}$) represented the N−H bending vibrations in adsorbed ammonia [59]. Several negative bands at 3622 and 3597 cm^{-1} were observed in the spectra. The band at 3622 cm^{-1} was due to the NH_3 adsorbed on P-OH groups [36]. The band at 3597 cm^{-1} was assigned to the stretching vibrations of the Al-OH-Si groups. Both of these bands are signatures of Brønsted acid sites [60].

In the N−H stretching region, the band at 3277 cm^{-1} could be assigned to ammonium ions, and the band at 3338 cm^{-1} may be assigned to NH_3 molecule adsorption [42]. The band at 3182 cm^{-1} was due to NH_3 absorbed on the Cu^+ sites of the catalyst [44,61–63]. In the N−H bending vibration region, the band at 1461 cm^{-1} corresponded to the bending vibration for NH_4^+, via NH_3 adsorbed on Brønsted acid sites (Si-OH, P-OH or bridging OH sites), while the bands at 1619 cm^{-1},

1275 cm^{-1} and 1225 cm^{-1} were all assigned to the NH_3 coordinated to Lewis acid sites [36,64]. The peak at 1619 cm^{-1} was assigned to Lewis acid sites associated with the exchanged Cu, and the 1275 and 1225 cm^{-1} peaks were attributed to Lewis acid sites on extra-framework Al^{3+} on zeolites [64,65] A negative band was detected at 894 cm^{-1}. The peak in this region was associated with the tetrahedral cation-oxygen-tetrahedral cation (T-O-T) framework vibrations that were perturbed by ion-exchanged copper species [42,44]. The change of peak intensity can be seen from the calculated integral areas of DRIFT spectra, as shown in Table 4. After H_2 reduction treatment and exposure to the SCR atmosphere, the bands at 1619 cm^{-1} became intense and the negative bands at 3622 and 3597 cm^{-1} were less intense, indicating that the number of surface Brønsted acid sites decreased and the number of Lewis acid sites increased, which may be due to more Cu ions substituting for the protons (Si-OH-Al) of the support, resulting in the transformation of Brønsted acid sites to Lewis acid sites [66].

3.4. Discussion

Cu/SAPO-18 had been prepared by adopting post-synthetic (ion-exchange and wetness impregnation) and one-pot methodologies via the use of commercially unavailable N, N-dimethyl-3, 5-dimethylpiperidinium [36,37,40]. The wetness impregnation method is much simpler and easier to scale up and the content of the metal cations is easier to control. During the impregnation, Cu cations could be introduced into the exchange site or form CuO_x species on the surface and in the channels of the zeolite. In this study, on the Cu/SAPO-18 obtained by the impregnation method, CuO_x species may be produced and block the pores of the zeolite, which resulted in the decline of the specific surface area and accumulated pore volume, as shown in the BET results (Table 1). Meanwhile, Cu cations were incorporated into the framework and cages of SAPO-18, so that the crystallinity decreased slightly and the interplanar crystal spacing of (110) significantly increased, as indicated by the XRD results (Fig. 1). The Cu/SAPO-18 catalyst was reduced by H_2 and then treated in the SCR atmosphere. As a result, the low-temperature performance was remarkably improved.

To understand the structure-activity relationships in Cu/SAPO-18-catalyzed SCR reactions and the effect of H_2 reduction treatment, the nature of Cu-containing species within the SAPO-18 framework must be discussed. There are three common forms of Cu species for Cu-zeolites: charge-balancing extra-framework Cu^{2+} monomers, charge-balancing $[Cu-O-Cu]^{2+}$ dimers and CuO_x clusters [67]. During the ion-exchange or impregnation process, $[Cu(OH)]^+$ may be formed and then dehydrated to form the Cu-dimer in the calcination process [68]. The diffraction peaks for CuO_x ($2\theta = 35.6°$ and $38.8°$) were not detected in the XRD profiles of these catalysts. This result illustrated that CuO_x species may highly disperse on the SAPO-18 support. The high-temperature activity of Cu/SAPO-18 decreased due to NH_3 unselective oxidation by CuO_x species.

The local chemistry of Cu species differed slightly within cation sites as a function of the presence of framework Al^{3+} in close proximity [18]. Gao et al. reported that Cu^{2+} would be exclusively located in the D6R sites of Cu-SSZ-13 when the Cu loading was low, but that Cu_2O_y would be formed in the 8-membered cage with the increase of Cu loading [53]. Verma et al. observed that Cu_xO_y species (per mole Cu, $x \geq 2$, $y \geq 1$) formed from the aggregation of isolated Cu^{2+} within the 8-membered cage in Cu-SSZ-13 (Si/Al = 4.5) with Cu/Al atomic ratio

Table 4
Integral areas of DRIFT spectra.

Samples	I^a (3597 cm^{-1})	I^a (3622 cm^{-1})	I^a (1619 cm^{-1})	I^a (894 cm^{-1})	Peak ratio (I_{894}/I_{3622})	Peak ratio (I_{894}/I_{1619})
Cu/SAPO-18	0.406	0.882	2.944	0.472	0.535	0.160
Cu/SAPO-18-R	0.151	0.474	3.413	0.415	0.875	0.121

[a] Integrated areas of DRIFT spectra after Kubelka-Munk conversion using OMNIC software.

limits above 0.2. The limit depended on the Si/Al atomic ratios of SSZ-13 [69]. For Cu/SAPO-18, ICP results showed that Si/Al was 0.57 and Cu/Al was 0.1. It was possible that Cu dimers formed within the 8-membered cages. Previous studies suggested that oxygen-bridged dimeric species, $[Cu-O-Cu]^{2+}$, which could be charge-compensated only by a pair of nearby Al sites, were the most probable catalytic SCR species in other Cu-exchanged zeolites, such as Cu-FAU and Cu-ZSM-5 [70–72]. From a statistical point of view, Al pairs could significantly present only in zeolites with a low Si/Al ratio [73]. In addition, UV–vis DRS was used to determine $[Cu-O-Cu]^{2+}$ dimer, and the results are shown in Fig. S3. The bands at 200–280 nm, 280–330 nm and 330–420 nm could be attributed to isolated Cu^{2+}, $[Cu-O-Cu]^{2+}$ dimer/CuO_x cluster and crystalline CuO_x, respectively [74,75]. Based on the above analysis, it could be expected that isolated Cu^{2+}, $[Cu-O-Cu]^{2+}$ and CuO_x clusters may exist in/on Cu/SAPO-18 catalyst.

Sarkany et al. confirmed that $[Cu-O-Cu]^{2+}$ species on the Cu-ZSM-5 were reduced more easily than isolated copper species, and $[Cu-O-Cu]^{2+}$ dimers could be reduced by H_2 to Cu^+ at 20 °C [68]. In the H_2-TPR profile, the H_2 consumption peak of Cu/SAPO-18 at 215 °C may be assigned to the reduction of $[Cu-O-Cu]^{2+}$ dimers. When Cu/SAPO-18 was treated by H_2 reduction at 250 °C, $[Cu-O-Cu]^{2+}$ dimers were reduced to Cu^+ ions, which were exchanged into SAPO-18 zeolite after exposure to the following NH$_3$-SCR atmosphere, just as in the solid-state ion-exchange methods [49]. Thus, more Cu^+ ions were detected in Cu/SAPO-18-R by H_2-TPR and XPS. During the H_2 treatment, Cu/SAPO-18-R may undergo lattice contraction and partial collapse of the zeolite framework because of the reduction of charge-compensated Cu dimers, in agreement with the XRD and BET results. In addition, the reduction of Cu dimers may produce H_2O, and Cu^{2+} may migrate in the moister atmosphere [53,76]. Therefore, the 'd' value (110) of Cu/SAPO-18-R decreased.

Cu^{2+}, $[Cu(OH)]^+$ and Cu^+ are all active centers in the SCR reaction, and the NH$_3$-SCR reaction occurs via the redox cycle between Cu^{2+} and Cu^+ [77]. Li et al. investigated the reasonable positions and coordination environment of active Cu sites in Cu/SAPO-18 catalysts by DFT calculation [36]. They found that the optimized and stable configuration was Cu^{2+} at the center of the D6R (hexagonal prisms) and the most unstable Cu^{2+} was located in the center of the pear-shaped cavity of SAPO-18, with the lowest relative stability energy. Paolucci et al. demonstrated that isolated Cu^{2+} first occupied these 2Al sites (D6R) before populating the remaining unpaired, or 1Al, sites as $[Cu^{2+}(OH)]^+$ (8-membered rings) in Cu-CHA [78]. In the H_2-TPR results of this study, there was only one peak at 252 °C assigned to Cu^{2+} in D6R sites in Cu/SAPO-18. After H_2 reduction treatment, another peak at 167 °C was found to be associated with the $[Cu^{2+}(OH)]^+$ within the cages of Cu/SAPO-18-R, which indicated that the migration of Cu species under the effects of H_2O or NH_3 took place during H_2 reduction and the NH$_3$-SCR atmosphere treatment process. The H_2-TPR result seemed to contradict the EPR results, where only one type of isolated Cu^{2+} was detected. This may be because the Cu/SAPO-18 and Cu/SAPO-18-R catalysts were not dehydrated in the EPR experiments.

The problem of identifying the real active state of copper during the catalytic reaction was even more complex when the reducing agent (ammonia) and oxygen were present together with NO. The adsorbate-driven relocation or restructuring of active sites during the catalytic reaction was related to the case of Cu-zeolites. Cu^{2+} species in these 8-membered rings were sensitive to the environment, and could migrate into adjacent cages to participate in the SCR reaction through solvation by H_2O or NH_3, and had the best SCR activity [78]. Gao et al. also proposed that the SCR reaction was catalyzed by $[Cu(OH)]^+$ located next to 8-membered rings [79]. Lomachenko et al. found that low-temperature SCR (< 200 °C) activity was determined by the ratio of Cu^+/Cu^{2+} sites and dominated by mobile NH$_3$-solvated Cu-species [80]. Paolucci et al. suggested that the low-temperature reaction rate depended on the Cu volumetric density, and NH$_3$-solvated Cu^+ ions were responsible for the standard SCR turnover [81]. Shwan et al. also

found that the mobility of Cu at low temperature was related to the formation of $[Cu^+(NH_3)_x]^+$ ($x \geq 2$) complexes [49]. Chen et al. indicated that Cu^+ ions made a major contribution to the low-temperature deNO$_x$ activity [54]. In the XPS and H_2-TPR results, the surface and bulk ratios of Cu^+/Cu^{2+} ions for Cu/SAPO-18-R were higher than those in Cu/SAPO-18, which may be the reason for the improvement in the low-temperature activity.

4. Conclusions

Copper species, such as isolated Cu^{2+}, Cu dimers and CuO_x clusters, existed in/on Cu/SAPO-18 catalysts. Firstly, Cu dimers were reduced to Cu^+ or $[Cu(OH)]^+$ by H_2 reduction treatment and then exchanged into the SAPO-18 zeolite under the NH$_3$-SCR atmosphere to generate more isolated Cu active centers for the standard SCR reaction. The low-temperature activity was related to balanced populations of Cu^+/Cu^{2+} sites and dominated by mobile NH$_3$-solvated Cu-species. In the low-temperature range, Cu ions could form transient ion pairs and move by NH$_3$ solvation, leading to the better activity. Therefore, H_2 reduction treatment and NH$_3$-SCR treatment broadened the operating temperature window of the standard SCR reaction for the Cu/SAPO-18 catalyst, and especially enhanced the low temperature activity.

Appendix A. Supplementary data

Supplementary data to this article can be found online at https://doi.org/10.1016/j.apsusc.2019.03.336.

References

[1] S. Roy, M.S. Hegde, G. Madras, Catalysis for NO$_x$ abatement, Appl. Energy 86 (2009) 2283–2297.

[2] V.I. Pavulescu, P. Grange, B. Delmon, Catalytic removal of NO, Catal. Today 46 (1998) 233–316.

[3] F. Liu, H. He, C. Zhang, Z. Feng, L. Zheng, Y. Xie, T. Hu, Selective catalytic reduction of NO with NH$_3$ over iron titanate catalyst: catalytic performance and characterization, Appl. Catal. B Environ. 96 (2010) 408–420.

[4] W. Shan, F. Liu, H. He, X. Shi, C. Zhang, An environmentally-benign CeO$_2$-TiO$_2$ catalyst for the selective catalytic reduction of NO$_x$ with NH$_3$ in simulated diesel exhaust, Catal. Today 184 (2012) 160–165.

[5] W. Xu, Y. Yu, C. Zhang, H. He, Selective catalytic reduction of NO by NH$_3$ over a Ce/TiO$_2$ catalyst, Catal. Commun. 9 (2008) 1453–1457.

[6] W. Shan, F. Liu, H. He, X. Shi, C. Zhang, A superior Ce-W-Ti mixed oxide catalyst for the selective catalytic reduction of NO$_x$ with NH$_3$, Appl. Catal. B Environ. 115–116 (2012) 100–106.

[7] J. Yu, Z. Si, M. Zhu, X. Wu, L. Chen, D. Weng, J. Zou, NH$_3$-SCR activity, hydrothermal stability and poison resistance of a zirconium phosphate/Ce$_{0.5}$Zr$_{0.5}$O$_2$ catalyst in simulated diesel exhaust. RSC Adv. 5 (2015) 83594–83599.

[8] J. Yu, Z. Si, L. Chen, X. Wu, D. Weng, Selective catalytic reduction of NO$_x$ by ammonia over phosphate-containing Ce$_{0.75}$Zr$_{0.25}$O$_2$ solids, Appl. Catal. B Environ. 163 (2015) 223–232.

[9] P.G. Smirniotis, D.A. Pena, B.S. Uphade, Low-temperature selective catalytic reduction (SCR) of NO with NH$_3$ by using Mn, Cr, and Cu oxides supported on Hombikat TiO$_2$, Angew. Chem. Int. Ed. 40 (2001) 2479–2482.

[10] Z. Liu, J. Zhu, J. Li, L. Ma, S.I. Woo, Novel Mn-Ce-Ti mixed-oxide catalyst for the selective catalytic reduction of NO$_x$ with NH$_3$, ACS Appl. Mater. Interfaces 6 (2014) 14500–14508.

[11] F. Liu, W. Shan, Z. Lian, L. Xie, W. Yang, H. He, Novel MnWO$_x$ catalyst with remarkable performance for low temperature NH$_3$-SCR of NO$_x$, Catal. Sci. Technol. 3 (2013) 2699–2707.

[12] G. Ramis, L. Yi, G. Busca, M. Turco, E. Kotur, R.J. Willey, Adsorption, activation, and oxidation of ammonia over SCR catalysts, J. Catal. 157 (1995) 523–535.

[13] Z. Si, D. Weng, X. Wu, J. Li, G. Li, Structure, acidity and activity of CuO$_x$/WO$_x$-ZrO$_2$ catalyst for selective catalytic reduction of NO by NH$_3$, J. Catal. 271 (2010) 43–51.

[14] S. Brandenberger, O. Krocher, A. Tissler, R. Althoff, The state of the art in selective

catalytic reduction of NO$_x$ by ammonia using metal-exchanged zeolite catalysts, Catal. Rev. 50 (2008) 492–531.

[15] R.Q. Long, R.T. Yang, Superior Fe-ZSM-5 catalyst for selective catalytic reduction of nitric oxide by ammonia, J. Am. Chem. Soc. 121 (1999) 5595–5596.

[16] J.H. Park, H.J. Park, J.H. Baik, I.S. Nam, C.H. Shin, J.H. Lee, B.K. Cho, S.H. Oh, Hydrothermal stability of Cu-ZSM-5 catalyst in reducing NO by NH$_3$ for the urea selective catalytic reduction process, J. Catal. 240 (2006) 47–57.

[17] J. Li, L. Jia, W. Jin, F. Xia, J. Wang, Effects of Ce-doping on the structure and NH$_3$-SCR activity of Fe/Beta catalyst, Rare Metal Mater. Eng. 44 (2015) 1612–1616.

[18] U. Deka, I. Lezcano-Gonzalez, B.M. Weckhuysen, A.M. Beale, Local environment and nature of Cu active sites in zeolite-based catalysts for the selective catalytic reduction of NO$_x$, ACS Catal. 3 (2013) 413–427.

[19] J. Wang, H. Zhao, G. Haller, Y. Li, Recent advances in the selective catalytic reduction of NO$_x$ with NH$_3$ on Cu-chabazite catalysts, Appl. Catal. B Environ. 202 (2017) 346–354.

[20] J.H. Kwak, R.G. Tonkyn, D.H. Kim, J. Szanyi, C.H.F. Peden, Excellent activity and selectivity of Cu-SSZ-13 in the selective catalytic reduction of NO$_x$ with NH$_3$, J. Catal. 275 (2010) 187–190.

[21] J.H. Kwak, D. Tran, S.D. Burton, J. Szanyi, J.H. Lee, C.H.F. Peden, Effects of hydrothermal aging on NH$_3$-SCR reaction over Cu/zeolites, J. Catal. 287 (2012) 203–209.

[22] D.W. Fickel, E. D'Addio, J.A. Lauterbach, R.F. Lobo, The ammonia selective catalytic reduction activity of copper-exchanged small-pore zeolites, Appl. Catal. B Environ. 102 (2011) 441–448.

[23] Z. Zhao, R. Yu, R. Zhao, C. Shi, H. Gies, F. Xiao, D. De Vos, T. Yokoi, X. Bao, U. Kolb, M. Feyen, R. McGuire, S. Maurer, A. Moini, U. Muller, W. Zhang, Cu-exchanged Al-rich SSZ-13 zeolite from organotemplate-free synthesis as NH$_3$-SCR catalyst: effects of Na$^+$ ions on the activity and hydrothermal stability, Appl. Catal. B Environ. 217 (2017) 421–428.

[24] L. Xie, F. Liu, X. Shi, F. Xiao, H. He, Effects of post-treatment method and Na co-cation on the hydrothermal stability of Cu-SSZ-13 catalyst for the selective catalytic reduction of NO$_x$ with NH$_3$, Appl. Catal. B Environ. 179 (2015) 206–212.

[25] L. Xie, F. Liu, L. Ren, X. Shi, F. Xiao, H. He, Excellent performance of one-pot synthesized Cu-SSZ-13 catalyst for the selective catalytic reduction of NO$_x$ with NH$_3$, Environ. Sci. Technol. 48 (2014) 566–572.

[26] Y.J. Kim, J.K. Lee, K.M. Min, S.B. Hong, I.S. Nam, B.K. Cho, Hydrothermal stability of CuSSZ13 for reducing NO$_x$ by NH$_3$, J. Catal. 311 (2014) 447–457.

[27] T. Zhang, H. Chang, Y. You, C. Shi, J. Li, Excellent activity and selectivity of one-pot synthesized Cu-SSZ-13 catalyst in the selective catalytic oxidation of ammonia to nitrogen, Environ. Sci. Technol. 52 (2018) 4802–4808.

[28] R. Zhang, J.S. McEwen, Local environment sensitivity of the Cu K-edge XANES features in Cu-SSZ-13: analysis from first-principles, J. Phys. Chem. Lett. 9 (2018) 3035–3042.

[29] Y. Jangjou, Q. Do, Y. Gu, L.G. Lim, H. Sun, D. Wang, A. Kumar, J. Li, L.C. Grabow, W.S. Epling, Nature of Cu active centers in Cu-SSZ-13 and their responses to SO$_2$ exposure, ACS Catal. 8 (2018) 1325–1337.

[30] P.S. Hammershoi, Y. Jangjou, W.S. Epling, A.D. Jensen, T.V.W. Janssens, Reversible and irreversible deactivation of Cu-CHA NH$_3$-SCR catalysts by SO$_2$ and SO$_3$, Appl. Catal. B Environ. 226 (2018) 38–45.

[31] F. Gao, C.H.F. Peden, Recent progress in atomic-level understanding of Cu/SSZ-13 selective catalytic reduction catalysts, Catalysts 8 (2018) 140, https://doi.org/10.3390/catal8040140.

[32] M. Moliner, C. Franch, E. Palomares, M. Grill, A. Corma, Cu-SSZ-39, an active and hydrothermally stable catalyst for the selective catalytic reduction of NO$_x$, Chem. Commun. 48 (2012) 8264–8266.

[33] N. Martin, C.R. Boruntea, M. Moliner, A. Corma, Efficient synthesis of the Cu-SSZ-39 catalyst for DeNO$_x$ applications, Chem. Commun. 51 (2015) 11030–11033.

[34] J. Chen, P.A. Wright, J.M. Thomas, S. Natarajan, L. Marchese, S.M. Bradley, G. Sankar, C.R.A. Catlow, P.L. Gaiboyes, R.P. Townsend, C.M. Lok, SAPO-18 catalysts and their Bronsted acid sites, J. Phys. Chem. 98 (1994) 10216–10224.

[35] A.G. Gayubo, R. Vivanco, A. Alonso, B. Valle, A.T. Aguayo, Kinetic behavior of the SAPO-18 catalyst in the transformation of methanol into olefins, Ind. Eng. Chem. Res. 44 (2005) 6605–6614.

[36] Y. Li, J. Deng, W. Song, J. Liu, Z. Zhao, M. Gao, Y. Wei, L. Zhao, Nature of Cu species in Cu-SAPO-18 catalyst for NH$_3$-SCR: combination of experiments and DFT calculations, J. Phys. Chem. C 120 (2016) 14669–14680.

[37] R. Martinez-Franco, M. Moliner, A. Corma, Direct synthesis design of Cu-SAPO-18, a very efficient catalyst for the SCR of NO$_x$, J. Catal. 319 (2014) 36–43.

[38] S. Ming, Z. Chen, C. Fan, L. Pang, W. Guo, K.B. Albert, P. Liu, T. Li, The effect of copper loading and silicon content on catalytic activity and hydrothermal stability of Cu-SAPO-18 catalyst for NH$_3$-SCR, Appl. Catal. A Gen. 559 (2018) 47–56.

[39] Z. Chen, C. Fan, L. Pang, S. Ming, W. Guo, P. Liu, H. Chen, T. Li, One-pot synthesis of high performance Cu-SAPO-18 catalyst for NO reduction by NH$_3$-SCR: influence of silicon content on the catalytic properties of Cu-SAPO-18, Chem. Eng. J. 348 (2018) 608–617.

[40] Y. Li, W. Song, J. Liu, Z. Zhao, M. Gao, Y. Wei, Q. Wang, J. Deng, The protection of CeO$_2$ thin film on Cu-SAPO-18 catalyst for highly stable catalytic NH$_3$-SCR performance, Chem. Eng. J. 330 (2017) 926–935.

[41] F. Gao, E.D. Walter, N.M. Washton, J. Szanyi, C.H.F. Peden, Synthesis and evaluation of Cu-SAPO-34 catalysts for ammonia selective catalytic reduction. 1. Aqueous solution ion exchange. ACS Catal. 3 (2013) 2083–2093.

[42] L. Wang, W. Li, G. Qi, D. Weng, Location and nature of Cu species in Cu/SAPO-34 for selective catalytic reduction of NO with NH$_3$, J. Catal. 289 (2012) 21–29.

[43] S. Fan, J. Xue, T. Yu, D. Fan, T. Hao, M. Shen, W. Li, The effect of synthesis methods on Cu species and active sites over Cu/SAPO-34 for NH$_3$-SCR reaction, Catal. Sci. Technol. 3 (2013) 2357–2364.

[44] L. Wang, J.R. Gaudet, W. Li, D. Weng, Migration of Cu species in Cu/SAPO-34 during hydrothermal aging, J. Catal. 306 (2013) 68–77.

[45] J. Xue, X. Wang, G. Qi, J. Wang, M. Shen, W. Li, Characterization of copper species over Cu/SAPO-34 in selective catalytic reduction of NO$_x$ with Ammonia: relationships between active cu sites and De-NO$_x$ performance at low temperature, J. Catal. 306 (2013) 56–64.

[46] M. Iwasaki, K. Yamazaki, K. Banno, H. Shinjoh, Characterization of Fe/ZSM-5 DeNO$_x$ catalysts prepared by different methods: relationships between active fe sites and NH$_3$-SCR performance, J. Catal. 260 (2008) 205–216.

[47] S. Shwan, J. Jansson, L. Olsson, M. Skoglundh, Effect of post-synthesis hydrogen-treatment on the nature of iron species in Fe-BEA as NH$_3$-SCR catalyst, Catal. Sci. Technol. 4 (2014) 2932–2937.

[48] R. Nedyalkova, S. Shwan, M. Skoglundh, L. Olsson, Improved lw-temperature SCR activity for Fe-BEA catalysts by H$_2$-pretreatment, Appl. Catal. B Environ. 138 (2013) 373–380.

[49] S. Shwan, M. Skoglundh, L.F. Lundegaard, R.R. Tiruvalam, A. Janssens, T.V.W. Carlsson, P.N.R. Vennestrøm, Solid-state ion-exchange of copper into zeolites facilitated by ammonia at low temperature, ACS Catal. 5 (2015) 16–19.

[50] D. Zhao, Y. Zhang, Z. Li, Y. Wang, J. Yu, Synthesis of SAPO-18/34 intergrowth zeolites and their enhanced stability for dimethyl ether to olefins, RSC Adv. 7 (2017) 939–946.

[51] L. Xu, A. Du, Y. Wei, Y. Wang, Z. Yu, Y. He, X. Zhang, Z. Liu, Synthesis of SAPO-34 with only Si(4Al) species: effect of Si contents on Si incorporation mechanism and Si coordination environment of SAPO-34, Microporous Mesoporous Mater. 115 (2008) 332–337.

[52] J. Wang, T. Yu, X. Wang, G. Qi, J. Xue, M. Shen, W. Li, The influence of silicon on the catalytic properties of Cu/SAPO-34 for NO$_x$ reduction by ammonia-SCR, Appl. Catal. B Environ. 127 (2012) 137–147.

[53] F. Gao, E.D. Walter, E.M. Karp, J. Luo, R.G. Tonkyn, J.H. Kwak, J. Szanyi, C.H.F. Peden, Structure-activity relationships in NH$_3$-SCR over Cu-SSZ-13 as probed by reaction kinetics and EPR studies, J. Catal. 300 (2013) 20–29.

[54] B. Chen, R. Xu, R. Zhang, N. Liu, Economical way to synthesize SSZ-13 with abundant ion-exchanged Cu$^+$ for an extraordinary performance in selective catalytic reduction (SCR) of NO$_x$ by Ammonia, Environ. Sci. Technol. 48 (2014) 13909–13916.

[55] J.H. Kwak, H. Zhu, J.H. Lee, C.H.F. Peden, S. J. Zanyi, Two different cation positions in Cu-SSZ-13? Chem. Commun. 48 (2012) 4758–4760.

[56] J. Wang, Y. Chen, L. Tang, W. Bao, L. Chang, L. Han, One-step hydrothermal synthesis of Cu-SAPO-34/cordierite and its catalytic performance on NO$_x$ removal from diesel vehicles, Trans. Nonferrous Metals Soc. China 26 (2013) 3330–3336.

[57] J. Wang, Z. Peng, H. Qiao, L. Han, W. Bao, L. Chang, G. Feng, W. Liu, Influence of aging on in situ hydrothermally synthesized Cu-SSZ-13 catalyst for NH$_3$-SCR reaction, RSC Adv. 4 (2014) 42403–42411.

[58] B.L. Meyers, T.H. Fleisch, G.J. Ray, J.T. Miller, J.B. Hall, A multitechnique characterization of dealuminated mordenites, J. Catal. 110 (1988) 82–95.

[59] H. Zhu, J.H. Kwak, C.H.F. Peden, J. Szanyi, In situ DRIFTS-MS studies on the oxidation of adsorbed NH$_3$ by NO$_x$ over a Cu-SSZ-13 zeolite, Catal. Today 205 (2012) 16–23.

[60] D. Wang, Y. Jangjou, Y. Liu, M.K. Sharma, J. Luo, J. Li, K. Kamasamudram, W.S. Epling, A comparison of hydrothermal aging effects on NH$_3$-SCR of NO$_x$ over Cu-SSZ-13 and Cu-SAPO-34 catalysts, Appl. Catal. B Environ. 165 (2015) 438–445.

[61] L. Ma, Y. Cheng, G. Cavataio, R.W. McCabe, L. Fu, J. Li, In situ DRIFTS and temperature-programmed technology study on NH$_3$-SCR of NO$_x$ over Cu-SSZ-13 and Cu-SAPO-34 catalysts, Appl. Catal. B Environ. 156-157 (2014) 428–437.

[62] D. Wang, L. Zhang, K. Kamasamudram, W.S. Epling, In situ-DRIFTS study of selective catalytic reduction of NO$_x$ by NH$_3$ over Cu-exchanged SAPO-34, ACS Catal. 3 (2013) 871–881.

[63] L. Wang, W. Li, S.J. Schmieg, D. Weng, Role of Bronsted acidity in NH$_3$ selective catalytic reduction reaction on Cu/SAPO-34 catalysts, J. Catal. 324 (2015) 98–106.

[64] L. Zhang, D. Wang, Y. Liu, K. Kamasamudram, J. Li, W. Epling, SO$_2$ poisoning impact on the NH$_3$-SCR reaction over a commercial Cu-SAPO-34 SCR catalyst, Appl. Catal. B Environ. 156-157 (2014) 371–377.

[65] F. Giordanino, E. Borfecchia, K.A. Lomachenko, A. Lazzarini, G. Agostini, E. Gallo, A.V. Soldatov, P. Beato, S. Bordiga, C. Lamberti, Interaction of NH$_3$ with Cu-SSZ-13 catalyst: a complementary FTIR, XANES, and XES study, J. Phys. Chem. Lett. 5 (2014) 1552–1559.

[66] X. Liu, X. Wu, D. Weng, Z. Si, R. Ran, Evolution of copper species on Cu/SAPO-34 SCR catalysts upon hydrothermal aging, Catal. Today 281 (2017) 596–604.

[67] G. Centi, S. Perathoner, Nature of active species in copper-based catalysts and their chemistry of transformation of nitrogen oxides, Appl. Catal. A Gen. 132 (1995) 179–259.

[68] J. Sárkány, J.L. D'Itri, W.M.H. Sachtler, Redox chemistry in excessively ion-exchanged Cu/Na-ZSM-5, Catal. Lett. 16 (1992) 241–249.

[69] A.A. Verma, S.A. Bates, T. Anggara, C. Paolucci, A.A. Parekh, K. Kamasamudram, A. Yezerets, J.T. Miller, W.N. Delgass, W.F. Schneider, F.H. Ribeiro, NO oxidation: a probe reaction on Cu-SSZ-13, J. Catal. 312 (2014) 179–190.

[70] M.N.T. Komatsu, I.S. Moon, T. Takahara, S. Namba, T. Yashima, Kinetic studies of reduction of nitric oxide with ammonia on Cu^{2+}-exchanged zeolites, J. Catal. 148 (1994) 427–437.

[71] S. Kieger, G. Delahay, B. Coq, B. Neveu, Selective catalytic reduction of nitric oxide by ammonia over Cu-FAU catalysts in oxygen-rich atmosphere, J. Catal. 183 (1999) 267–280.

[72] G.M. Psofogiannakis, J.F. McCleerey, E. Jaramillo, A.C.T. van Duin, ReaxFF reactive molecular dynamics simulation of the hydration of Cu-SSZ-13 zeolite and the formation of Cu dimers, J. Phys. Chem. C 119 (2015) 6678–6686.

[73] F. Giordanino, P.N.R. Vennestrøm, L.F. Lundegaard, F.N. Stappen, S. Mossin,

P. Beato, S. Bordiga, C. Lamberti, Characterization of Cu-exchanged SSZ-13: a comparative FTIR, UV-Vis, and EPR study with Cu-ZSM-5 and Cu-β with similar Si/Al and Cu/Al ratios, Dalton Trans. 42 (2013) 12741–12761.

[74] M.C.N. Amorim de Carvalho, F.B. Passos, M. Schmal, The behavior of Cu/ZSM-5 in the oxide and reduced form in the presence of NO and methanol, Appl. Catal. A Gen. 193 (2000) 265–276.

[75] D. Jo, G. Park, T. Ryu, S.B. Hong, Economical synthesis of high-silica LTA zeolites: a step forward in developing a new commercial NH_3-SCR catalyst, Appl. Catal. B Environ. 243 (2019) 212–219.

[76] F. Gao, J. Kwak, J. Szanyi, C.F. Peden, Current understanding of Cu-exchanged chabazite molecular sieves for use as commercial diesel engine $DeNO_x$ catalysts, Top. Catal. 56 (2013) 1441–1459.

[77] V.F. Kispersky, A.J. Kropf, F.H. Ribeiro, J.T. Miller, Low absorption vitreous carbon reactors for operando XAS: a case study on Cu/zeolites for selective catalytic reduction of NO_x by NH_3, Phys. Chem. Chem. Phys. 14 (2012) 2229–2238.

[78] C. Paolucci, A.A. Parekh, I. Khurana, J.R. Di Iorio, H. Li, J.D. Albarracin Caballero, A.J. Shih, T. Anggara, W.N. Delgass, J.T. Miller, F.H. Ribeiro, R. Gounder, W.F. Schneider, Catalysis in a cage: condition-dependent speciation and dynamics of exchanged Cu cations in SSZ-13 zeolites, J. Am. Chem. Soc. 138 (2016) 6028–6048.

[79] F. Gao, E.D. Walter, M. Kollar, Y. Wang, J. Szanyi, C.H.F. Peden, Understanding ammonia selective catalytic reduction kinetics over Cu/SSZ-13 from motion of the Cu ions, J. Catal. 319 (2014) 1–14.

[80] K.A. Lomachenko, E. Borfecchia, C. Negri, G. Berlier, C. Lamberti, P. Beato, H. Falsig, S. Bordiga, The Cu-CHA $deNO_x$ catalyst in action: temperature-dependent NH_3-assisted selective catalytic reduction monitored by operando XAS and XES, J. Am. Chem. Soc. 138 (2016) 12025–12028.

[81] C. Paolucci, I. Khurana, A.A. Parekh, S.C. Li, A.J. Shih, H. Li, J.R. Di Iorio, J.D. Albarracin-Caballero, A. Yezerets, J.T. Miller, W.N. Delgass, F.H. Ribeiro, W.F. Schneider, R. Gounder, Dynamic multinuclear sites formed by mobilized copper ions in NO_x selective catalytic reduction, Science 357 (2017) 898–903.